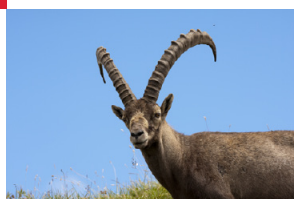

Abstract Volume
9th Swiss Geoscience Meeting

Zurich, 11th – 13th November 2011

21. Geophysics and Rockphysics

sc | nat

Geosciences
Platform of the Swiss Academy of Sciences

ETH
Eidgenössische Technische Hochschule Zürich
Swiss Federal Institute of Technology Zurich

21. Geophysics and Rockphysics

Marcel Frehner

Swiss Geophysical Commission

TALKS:

21.1 *Gabriel A.-A., Ampuero J.-P., Dalguer L. A., Mai P. M.:* Macroscopic Source Properties from Dynamic Rupture Simulations in Plastic Media

21.2 *Girard L., Gruber S., Weber S., Amitrano D.:* Rock damage inferred from acoustic emissions in a partly frozen high-alpine rock-wall

21.3 *Kuteynikova M., Quintal B., Tisato N.:* Numerical modelling and laboratory measurements of seismic attenuation

21.4 *Madonna C., Almqvist B. S.G., Saenger E. H.:* Digital rock physics: numerical prediction of pressuredependent ultrasonic velocities using micro-CT imaging

21.5 *Quintal B., Steeb H., Frehner M., Schmalholz S.M.:* S-wave attenuation due to wave-induced fluid flow in heterogeneous, partially saturated porous media

21.6 *Riahi N., Birkelo B., Saenger E. H.:* A statistical approach to ambient wave field analysis

21.7 *Saenger E.H., Enzmann F., Keehm Y., Steeb H.:* Digital rock physics: Effect of fluid viscosity on effective elastic properties

21.8 *van Dinther Y., Gerya T.V., Corbi F., Funiciello F., Mai P.M., Dalguer L.A.:* The long-term seismic cycle at subduction thrusts: benchmarking geodynamic numerical simulations and analogue mode

POSTERS:

P 21.1 *Abdelfettah Yassine, Schill Eva:* Accurate gravity data correction and 3D gravity forward modeling

P 21.2 *Almqvist B.S.G, Aschwanden L., Diamond L., Ramseyer K., Zappone A.:* Characterization of the Upper Muschelkalk aquifer in northeast Switzerland using laboratory physical properties and imaging techniques

P 21.3 *Baumann C.F.D., Dalguer L.A.:* Toward source characterization of local supershear ruptures in dip-slip faults

P 21.4 *Benson, P., Heap, M., Lavallée, Y., Flaws, A., Hess, K., Cordonnier, B. and Misra, S.:* Laboratory simulations of tensile (hydro) fracture: current work and new directions

P 21.5 *Frehner M., Quintal B.:* Physical mechanisms for low-frequency seismic wave attenuation in fractured media

P 21.6 *Kaveh Khaksar, Marahem Rahmati:* Rock classification based on physico-mechanical analysis -case study: Poshtkuh basin, Alborze region-Iran

P 21.7 *Madonna C., Tisato N., Saenger E. H.:* Low frequency measurements of seismic wave attenuation

P 21.8 *Schoenball, M., Baujard, C, Kohl, T., Dorbath, L.:* Changes of Coulomb Failure Stress due to Dislocations during Stimulation of GPK2 at Soultz-sous-Forêts

P 21.9 *Tisato N., Madonna C., Saenger E.H.:* Measurements and mechanisms of seismic wave attenuation in partially saturated rocks

P 21.10 *Zappone A.., Bruijn R., Tripoli B., Biedermann A.R., Burg J-P., Kissling E.:* The Swiss Atlas of Physical Properties of Rocks (SAPHYR): Progress and developments

P 21.11 *Zappone A., Diamond L., Almqvist B., Evans K., Deichmann N., Werner M., Mazzotti M.:* Carma – Carbon Management in Power Generation: Geological CO_2 storage in Switzerland

21.1

Macroscopic Source Properties from Dynamic Rupture Simulations in Plastic Media

Gabriel Alice-Agnes[1], Ampuero Jean-Paul[2], Dalguer Luis Angel[1], Mai Paul Martin[3]

[1]*Swiss Seismological Service, ETH Zurich, Sonneggstr. 5, CH-8032 Zurich, Switzerland (alice@sed.ethz.ch)*
[2]*Seismological Laboratory, California Institute of Technology, 1200 E. California Blvd., MC 252-21, Pasadena, CA 91125, USA*
[3]*Division of Physical Sciences & Engineering, King Abdullah University of Science and Technology, Thuwal 23955-6900, Kingdom of Saudi Arabia*

High stress concentrations at earthquake rupture fronts may generate an inelastic off-fault response at the rupture tip, leading to increased energy absorption in the damage zone. Furthermore, the induced asymmetric plastic strain field in in-plane rupture modes may produce bimaterial interfaces that can increase radiation efficiency and reduce frictional dissipation. Off-fault inelasticity thus plays an important role for realistic predictions of near-fault ground motion.

Guided by our previous studies in the 2D elastic case, we perform rupture dynamics simulations including rate-and-state friction and off-fault plasticity to investigate the effects on the rupture properties. We quantitatively analyze macroscopic source properties for different rupture styles, ranging from cracks to pulses and subshear to supershear ruptures, and their transitional mechanisms. The energy dissipation due to off-fault inelasticity modifies the conditions to obtain each rupture style and alters macroscopic source properties. We examine apparent fracture energy, rupture and healing front speed, peak slip and peak slip velocity, dynamic stress drop and size of the process and plastic zones, slip and plastic seismic moment, and their connection to ground motion. This presentation focuses on the effects of rupture style and off-fault plasticity on the resulting ground motion patterns, especially on characteristic slip velocity function signatures and resulting seismic moments.

We aim at developing scaling rules for equivalent elastic models, as function of background stress and frictional parameters, that may lead to improved "pseudo-dynamic" source parameterizations for ground-motion calculation. Moreover, our simulations might provide quantitative relations between off-fault energy dissipation and macroscopic source properties.

21.2

Rock damage inferred from acoustic emissions in a partly frozen high-alpine rock-wall

Girard Lucas[1], Gruber Stephan[1], Weber Samuel[1] & Amitrano David[2]

[1] *3G, Dep. of Geography, University of Zurich, Winterthurerstr. 190, CH-8057 Zurich, Switzerland. (girard@geo.uzh.ch)*
[2] *ISTerre, CNRS - Université Joseph Fourier, Grenoble, BP 53, 38041 Grenoble Cedex 9, France.*

The formation of ice within rock is an important driver of rock damage near the surface and up to several meters depth. In steep terrain, this process may be crucial for the slow preconditioning of rock fall from warming permafrost areas. This presentation reports results from a pilot study where acoustic emission monitoring was used to investigate rock damage in a high-alpine rock-wall induced by natural thermal cycling and freezing/thawing.

Laboratory experiments as well as theoretical studies have contributed to clarify the basic mechanisms through which ice formation can damage rock: (i) the difference in density between the liquid water and the ice crystal, which results in the initial build-up of an in-pore pressure at the onset of crystallization and (ii) the cryo-suction process, which drives liquid water towards already frozen pores as the temperature further decreases. However, the transfer of corresponding theoretical insight and laboratory evidence to natural conditions characterized by strong spatial and temporal heterogeneity is nontrivial. The pilot experiment that we present here is intended to prepare the corresponding characterization of rock damage in natural conditions. The measurements were performed on a rock-wall located close to Jungfraujoch (Berner Oberland) at 3500m a.s.l. during 4 days in April 2010.

The results demonstrate the feasibility of such a technique: (i) the statistical properties of the acoustic emission events are shown to obey robust power-law distributions in the time and energy domains, expressing that rock damage and micro-fracturing are induced by stresses arising from thermal variations and associated freezing/thawing of rock; (ii) liquid water availability and rock temperature affect the acoustic emission activity, indicating the importance of freezing-induced stresses. These results suggest that the framework of further modeling studies (theoretical and numerical) should include damage, elastic interactions and poro-mechanics in order to describe freezing-related stresses.

21.3

Numerical modeling and laboratory measurements of seismic attenuation

Maria Kuteynikova[1], Beatriz Quintal[1], and Nicola Tisato[1]

[1]*The Rock Physics Network at ETH Zurich (ROCKETH), Sonneggstrasse 5, CH-8092 Zurich, Switzerland (maria.kuteynikova@erdw.ethz.ch)*

Estimating pore fluid properties of saturated porous rocks from seismic data is very important in exploration geophysics for finding hydrocarbon reservoirs and in reservoir geophysics for monitoring and optimizing production. Theoretical studies show that pore fluid properties have a major effect on attenuation and velocity dispersion of seismic waves. This effect opens the potential of estimating fluid properties from seismic data. However, despite years of research on this subject, this link has not yet been exploited by the oil industry in exploration and production routines. For that to happen, the effect of fluid properties on seismic attenuation and velocity dispersion has to be quantified and better understood through laboratory and numerical investigations.

A major cause of attenuation and velocity dispersion in the frequency range of interest in seismic exploration (1-100 Hz) is wave-induced flow of pore fluid in the mesoscopic scale (e.g., Pride et al., 2004). The mesoscopic scale is much larger than the pore size (2-50 nm) and much smaller than the seismic wavelengths (hundreds of meters for seismic frequencies). In White's model (White, 1975) a partially saturated rock can be approximated by a medium with mesoscopic-scale heterogeneities fully saturated with one fluid and the background fully saturated with anther fluid (so-called patchy saturation). The passing wave induces different fluid pressure in the regions saturated with fluids of different compressibilities.

Attenuation arises due to induced pressure gradients on the mesoscale, which causes fluid to flow and thus the loss of energy. White's model can be modeled using Biot's equations for wave propagation in poroelastic media with spatially varying petrophysical parameters. However, solving Biot's equations for wave propagation to calculate seismic attenuation due to wave-induced fluid flow is computationally inefficient because wave propagation and fluid flow occur on very different time scales. A method that is computationally efficient in calculating attenuation related to the fluid flow in the mesoscopic-scale is a quasi-static creep test (Masson and Pride, 2007). Furthermore, for calculating attenuation due to only wave-induced fluid flow at low seismic frequencies, inertial forces are negligible. Thus it is enough to solve a simpler mathematical problem, that is, Biot's equations of consolidation (Quintal et al., 2011).

In this work attenuation and velocity dispersion in porous saturated rocks due to wave-induced fluid flow are calculated by solving Biot's equations of consolidation with the software COMSOL. The finite element method is employed to simulate a creep test on a 2D numerical rock sample with mesoscopic-scale heterogeneities in fluid saturation. The resulting time-dependent stress-strain relations are transformed to the frequency domain with a fast Fourier transform and then used to calculate the undrained bulk and shear moduli. With these moduli, we determine the frequency-dependent P- and S-wave attenuation and velocity dispersion in the sample caused by the mechanism of wave-induced fluid flow.

Numerical modeling is useful to better understand the effect of rock-fluid properties on seismic waves. However, more than one physical mechanisms and complicated geometries and distributions of heterogeneities take place in real rocks. Thus, modeling needs a continuous comparison with laboratory data. Here we compare our numerical results to the data obtained using the Broad Band Attenuation Vessel (BBAV) (Tisato et al., 2011). The BBAV measures the phase angle between the force applied and the shortening of the sample, from which seismic wave attenuation at low frequencies (0.1-100 Hz) is calculated. The vessel can confine the sample, a cylinder of 0.25 m length and 0.038 m diameter, up to a pressure of 25 MPa to simulate subsurface in situ conditions. Attenuation (1/Q) measurements for two Berea sandstone samples with different permeability (about 300 and 800 mD), saturated with 90% water and 10% air, are shown in the figure below. The same physical parameters were imput into the numerical model. Solid lines show the numerical results for different geometries and patch size, but the same saturation (90% water). As we see, different sizes of patches have an influence on the frequency-dependent attenuation. Further studies are needed in order to fit and understand the attenuation curves obtained in the laboratory.

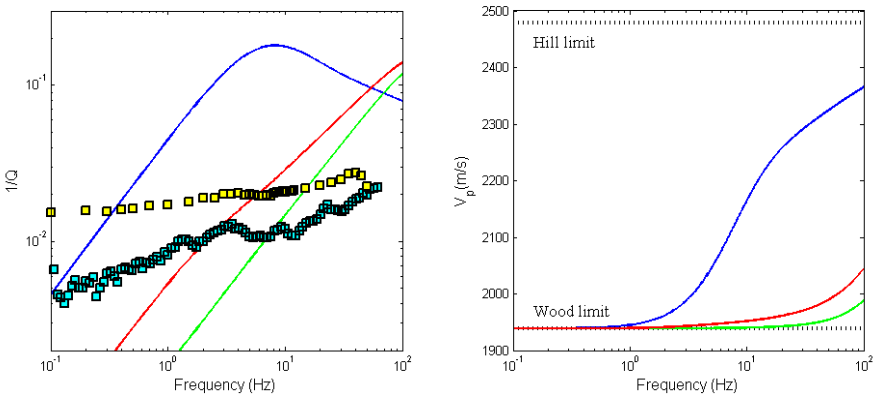

Figure 1. Numerical (solid lines) and laboratory (squares) results for attenuation (1/Q), and numerical results for the phase velocity (V_p), versus frequency. Phase velocities reach the Hills limit at higher frequencies.

REFERENCES

Masson, Y.J., and Pride, S.R., 2007, Poroelastic finite-difference modeling of seismic attenuation and dispersion due to mesoscopic-scale heterogeneity: Journal of Geophysical Research, 112, B03204.

Pride, S.R., Berryman, J.G., and Harris, J.M., 2004, Seismic attenuation due to wave-induced flow: Journal of Geophysical Research, 109, B01201.

Quintal, B., Steeb, H., Frehner, and M., Schmalholz, S.M., 2011, Quasi-static finite element modeling of seismic attenuation and dispersion due to wave-induced fluid flow in poroelastic media: Journal of Geophysical Research, 116, B01201.

Tisato, N., Madonna, C., Artman, B., and Saenger, E.H., 2011, Low frequency measurements of seismic wave attenuation in Berea sandstone: SEG International Exposition and 81st Annual Meeting.

White, J.E., 1975, Computed seismic speeds and attenuation in rocks with partial gas saturation: Geophysics, 40, 2.

21.4

Digital rock physics: numerical prediction of pressure-dependent ultrasonic velocities using micro-CT imaging

Madonna Claudio[1], Almqvist Bjarne S. G.[1] and Saenger Erik H.[1]

[1] *Geologisches Institut, Sonneggstrasse 5, CH-8092 Zürich (claudio.madonna@erdw.ethz.ch)*

Over the last decade, micro-tomography has rapidly evolved to become a common microscopy tool in the geosciences. Digital rock physics combines modern microscopic imaging with advanced numerical simulations for analysis of the physical properties of rocks, complementing laboratory investigations. X-ray micro-computed tomography (micro-CT) is among the emerging techniques used for digital rock physics. It allows analysis of a representative sample volume in a non-destructive way and enables the reconstruction of a realistic virtual 3D model of a porous material. Indeed, 3D micro-CT imaging and subsequent numerical determination of petrophysical properties have been applied in several studies, as well as the calculation of transport properties. Elastic-wave propagation modelling based on the microstructure images is used to estimate the effective elastic properties (Saenger et al. 2011).

As with every microscopic imaging technique, there is a trade-off between the maximum resolution and the investigated volume. Because a representative volume of a porous rock is imaged using the micro-CT technique, the smallest pores, micro-cracks, and grain-to-grain contacts remain unresolved. Such micro-structures may significantly influence the mechanical properties of a rock. For example, the elastic properties of granular material strongly depend on the grain-to-grain contacts which micro-CT imaging may not resolve.

The goal of this paper is to describe and understand how laboratory measurements of ultrasonic P-wave velocities compare with digital rock physics results based on the geometric microstructural details present in segmented micro-CT images. Using grain boundary reconstruction algorithms, we present a method for calibrating the numerically overestimated effective elastic properties based on experimental data obtained from a sample of Berea sandstone. We also suggest a strategy to predict pressure-dependent velocity using micro-CT images. A workflow is delineated that enables the identification of grain-to-grain contacts in the micro-CT images and, based on the laboratory calibration, the assignment of weaker micromechanical properties to the grain contacts for the subsequent numerical modeling.

REFERENCES

Saenger E.H., Enzmann F., Keehm Y. and Steeb H., 2011: Digital rock physics: Effect of fluid viscosity on effective elastic properties, Journal of Applied Geophysics 74, 236–241.

21.5

S-wave attenuation due to wave-induced fluid flow in heterogeneous, partially saturated porous media

Beatriz Quintal[1], Holger Steeb[2], Marcel Frehner[1], and Stefan M. Schmalholz[3]

[1]*The Rock Physics Network at ETH Zurich (ROCKETH), Sonneggstrasse 5, 8092, Zurich, Switzerland (beatriz.quintal@erdw.ethz.ch; marcel.frehner@erdw.ethz.ch)*
[2]*Ruhr-University Bochum, Bochum, Germany (holger.steeb@rub.de)*
[3]*University of Lausanne, Lausanne, Switzerland (stefan.schmalholz@unil.ch)*

We study seismic S-wave attenuation caused by wave-induced fluid flow at the mesoscopic scale (Pride et al., 2004). Simple-shear relaxation experiments are performed by solving Biot's (1941) equations for consolidation of 2D poroelastic media with finite-element modelling (Quintal et al., 2011). The experiments yield time-dependent stress-strain relations used to calculate the undrained shear modulus, from which S-wave attenuation is determined. Our model consists of periodically distributed (simple-cubic packing) circular heterogeneities with much lower porosity and permeability than the conti-

nuous background medium. The continuous background is fully saturated with oil and the low porosity regions are saturated with water. The background contains 80% of the total pore space of the medium. The total saturation in the medium is then 80% oil, 20% water. Snapshots of the relaxation experiment are shown in Figure 1.

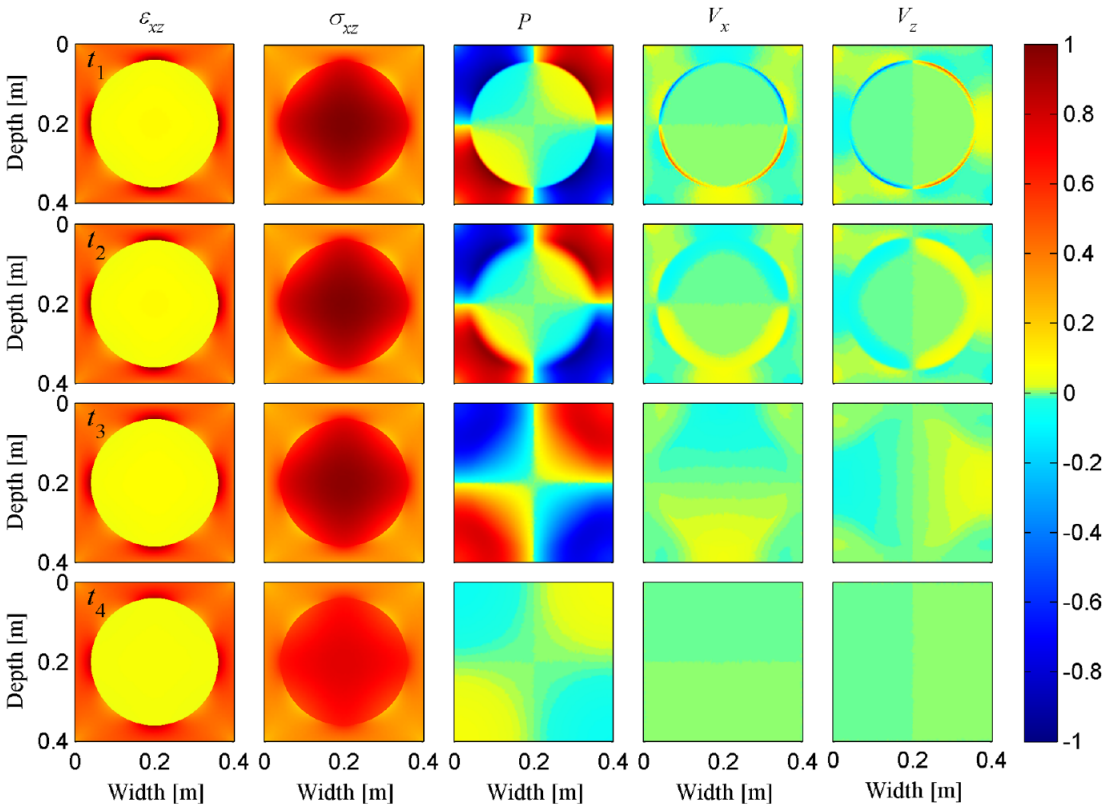

Figure 1. Snapshots at times t_1 = 8.66×10^{-6} s, t_2 = 1.15×10^{-4} s, t_3 = 2.8×10^{-3} s, and t_4 = 0.1 s, of the simple-shear relaxation experiment on the representative elementary volume with a circular heterogeneity saturated with oil. The fields ε_{xz} (shear strain), σ_{xz} (shear stress), P (pore fluid pressure), V_x and V_z (fluid velocity in the x- and z-directions) are normalized by their maximum values. The results are shown in Figure 2 (case A, oil-saturated heterogeneity).

For comparison, we also perform experiments for the background saturated with gas or water, instead of oil. The results are shown in Figure 2, where cases A to D differ in the values of the dry bulk and shear moduli (K and μ, respectively) in the background and in the heterogeneities. In case A, K and μ are, respectively, 36 and 32 GPa in the heterogeneity, and 4 and 2 GPa in the background. In case B, 36 and 32 GPa in the heterogeneity, 14 and 12 GPa in the background. In case C, 12 and 8 GPa in the heterogeneity, 4 and 2 GPa in the background. Case D is the opposite of case A, where K and μ are 4 and 2 GPa in the heterogeneity, and 36 and 32 GPa in the background.

The S-wave attenuation in this study is caused by flow of the pore fluid between the heterogeneity and the background caused by fluid pressure differences (see snapshots for P, V_x and V_z in Figure 1). A consistent tendency is observed in the relative behavior of the S-wave attenuation among the different saturation cases (Figure 2). First, in the gas-saturated media the S-wave attenuation is very low and much lower than in the oil-saturated or in the fully water-saturated media. Second, at low frequencies, the S-wave attenuation is significantly higher in the oil-saturated media than in the fully water-saturated media. Based on these tendencies, we suggest that S-wave attenuation could be used in seismic interpretation as an indicator and discriminator of fluid content in a reservoir, in addition to P-wave attenuation.

REFERENCES

Biot, M. A., 1941: General theory of three-dimensional consolidation: Journal of Applied Physics 12, 155-164.

Pride, S. R., J. G. Berryman, and J. M. Harris, 2004: Seismic attenuation due to wave-induced flow: Journal of Geophysical Research 109, B01201.

Quintal, B., H. Steeb, M. Frehner, and S. M. Schmalholz, 2011: Quasi-static finite element modeling of seismic attenuation and dispersion due to wave-induced fluid flow in poroelastic media: Journal of Geophysical Research – Solid Earth 116, B01201.

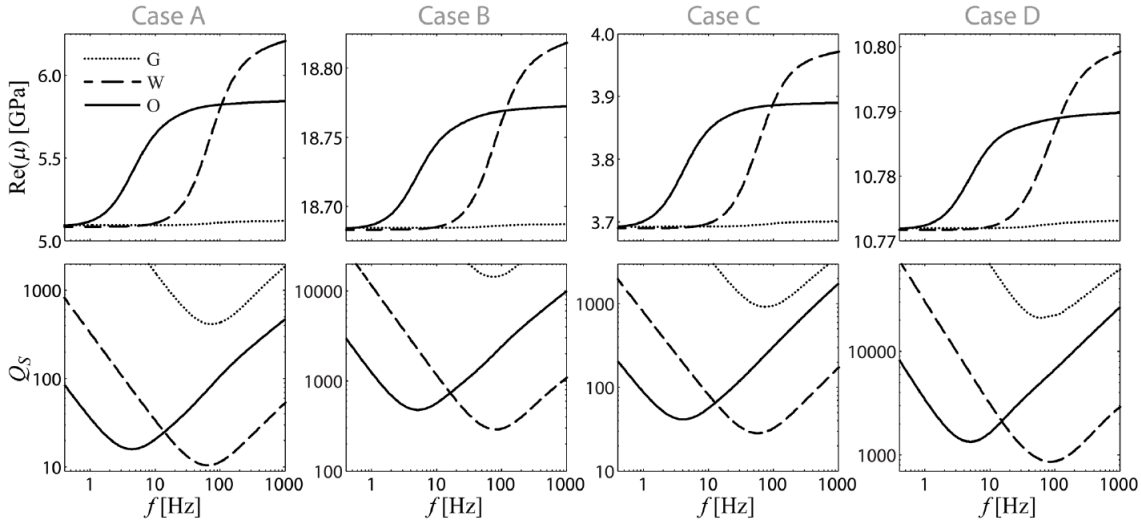

Figure 2. Numerical results for the real part of the undrained shear modulus, μ, and the S-wave quality factor, Q_s. The inverse of Q_s is a measure of S-wave attenuation. The legend terms refer to the fluid in the background: gas (G); water (W); or oil (O).

21.6

A statistical approach to ambient wave field analysis

Riahi Nima[1], Bradley Birkelo[2], Saenger Erik H.[1,2]

[1] *Earth Science Department ETH, Soneggstrasse 5, 8092 Zürich (nima.riahi@erdw.ethz.ch)*
[2] Spectraseis, 1899 Wynkoop Street, Denver CO 80202, United States

The ubiquitous ambient seismic wave field at the surface can be used to estimate earthquake site response, monitor oceanic weather, and image the Earth's crust. It is also hypothesized to interact with hydrocarbon reservoirs at >800 m depth and exhibit seismic power variations, in particular on the vertical component (Saenger et al., 2009). Attempts to empirically validate this hypothesis require observed correlations between passive seismic power attributes and a reservoir but also a careful investigation of potential confounders such as shallow geologic structure, water table, seismic surface noise sources, and the overburden (Hanssen & Bussat, 2008; Ali et al., 2010).

To test the hypothesis a measurement campaign was conducted at Europe's second largest underground gas storage (UGS) facility in Chémery, France. In two surveys in April and November 2011 about 120 three-component, broadband particle velocity sensors were deployed over several days above and around the UGS. The reservoir is expected to exhibit the largest saturation and pressure changes between these two time snapshots. In the planned time-lapse analysis the constant overburden cannot act as a confounder. However, seasonal variations of the water table and surface noise sources (farming, ocean storms, local weather) must be considered.

We present a three-stage statistical approach that aids in identifying frequency ranges where neither single surface sources dominate nor changes in the near-surface are evident. These tests constitute minimal requirements to pass before analyzing potential correlations to reservoir structures. First, transient and/or high-power noise sources such as traffic and earthquakes are removed by selecting only the 10% of time periods with lowest seismic power (Riahi et al., 2011). Second, the distribution of the azimuth of the dominant polarization of these time periods is tested for isotropy to exclude the possibility that a small number of surface sources was dominating the recording. Lastly, H/V-ratio spectra (Bonnefoy-Claudet, 2006) between the two time snapshots are compared to test if the shallow subsurface was constant, thereby reducing the likelihood of near-surface effects.

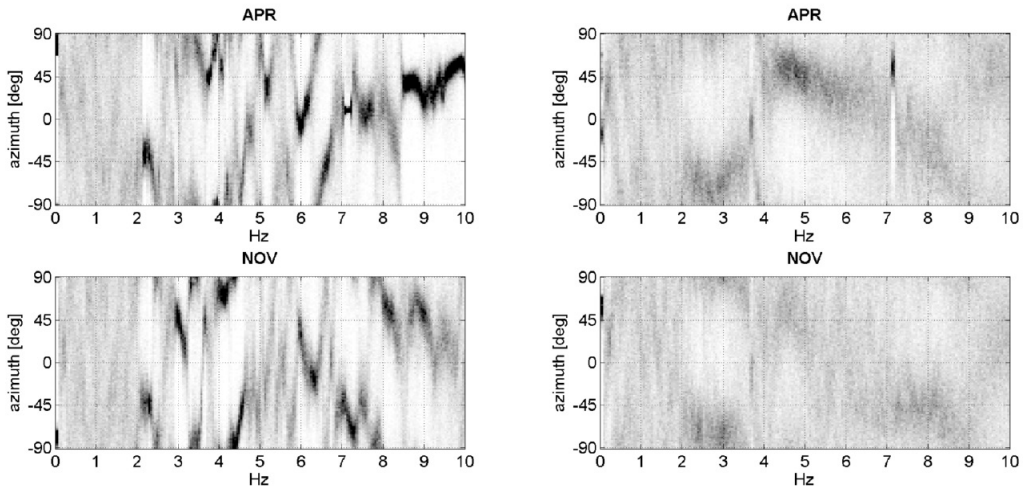

Figure 1 The distribution of polarization azimuth for a receiver near the surface-projected crest of the UGS (left hand side) and away from the UGS (right hand side). The top and bottom panels compare the situation between April and November. All panels reveal an isotropic particle motion below 2 Hz.

The method is illustrated on two sites selected from a larger set of measured locations. The example sites were situated away from the surface-projected crest of the UGS but above the gas storage and above a geologically similar, but gas-free aquifer. For these two particular sites the ambient wave field was found to be laterally isotropic below 2 Hz (Figure 1). Near-surface changes are unlikely to have affected that low-frequency band, as evidenced by stable H/V-spectra (Figure 2). The suggested tests can be applied to all measurements that are considered for a differential analysis to the reservoir.

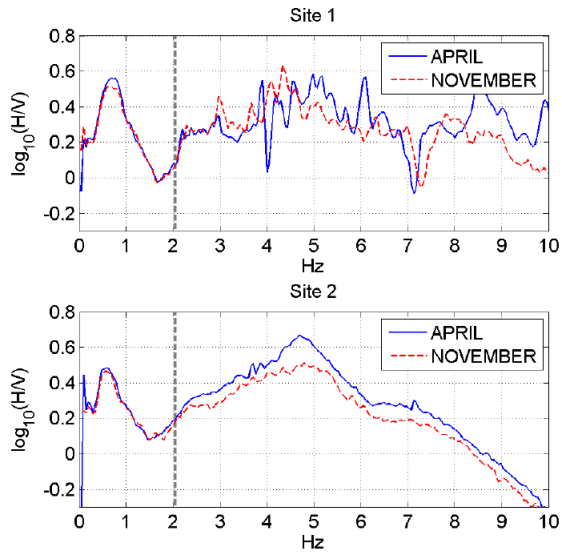

Figure 2 Comparison of H/V spectra observed in April and November for the location above the gas storage (top) and the aquifer (bottom). Below 2 Hz the spectral ratio is constant between the snapshots.

REFERENCES

Ali, M. Y., Berteussen K. A., Small J., and Barkat B. 2010: Low-frequency passive seismic experiments in Abu Dhabi, United Arab Emirates: implications for hydrocarbon detection, Geophys Prospect, 58(5), 875-899.

Bonnefoy-Claudet, S., Cotton F., and Bard P.-Y. 2006: The nature of noise wavefield and its applications for site effects studies: A literature review, Earth Science Reviews, 79, 205-227.

Hanssen, P., and Bussat S. 2008: Pitfalls in the analysis of low-frequency passive seismic data, First Break, 26, 111-119.

Riahi, N., Birkelo B., and Saenger E. H. 2011: Analyzing passive seismic attributes: a statistical strategy, paper presented at SEG Technical Program Expanded Abstracts, San Antonio.

Saenger, E. H., Schmalholz S. M., Lambert M. A., Nguyen T. T., Torres A., Metzger S., Habiger R. M., Muller T., Rentsch S., and Mendez-Hernandez E. 2009: A passive seismic survey over a gas field: Analysis of low-frequency anomalies, Geophysics, 74(2), O29-O40.

21.7

Digital rock physics: Effect of fluid viscosity on effective elastic properties

Erik H. Saenger[1], Frieder Enzmann[2], Youngseuk Keehm[3], Holger Steeb[4]

[1]*ETH Zurich and Spectraseis, Switzerland (erik.saenger@erdw.ethz.ch)*
[2]*Gutenberg-Universität Mainz, Germany*
[3]*Kongju National University, South Korea*
[4]*Ruhr-Universität Bochum, Germany*

This paper is concerned with the effect of pore fluid viscosity on effective elastic properties using digitized rocks. We determine a significant velocity dispersion in wave propagation simulations by the variation of the pore fluid viscosity (Figure 1). Several attenuation regimes are considered which may contribute to this observation. Starting point is a virtual rock physics approach. Numerical simulations of effective transport and effective mechanical properties are applied to statistically representative rock samples. The rock microstructure is imaged by 3D X-ray tomography. Permeability values were estimated through Lattice-Boltzmann flow simulations. The dry rock moduli and the tortuosity are derived by dynamic wave propagation simulations (Figure 2). We apply a displacement-stress rotated staggered finite-difference grid technique to solve the elastodynamic wave equation. An accurate approximation of a Newtonian fluid is implemented in this technique by using a generalized Maxwell body. We give a practical description of how to use this approach and discuss the application limits. Additionally, we show the simulated signature of a theoretically predicted slow S-wave.

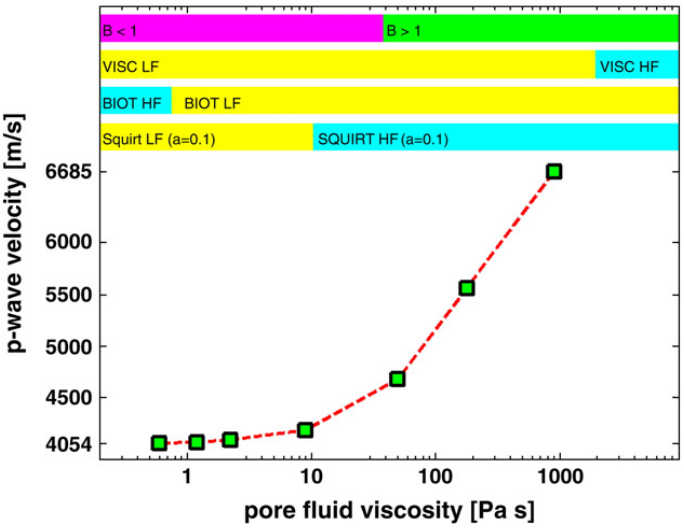

Figure 1. Numerically measured velocity vs. viscosity of the saturating fluid. Details of the corresponding simulations can be found in Saenger et al. (2011)

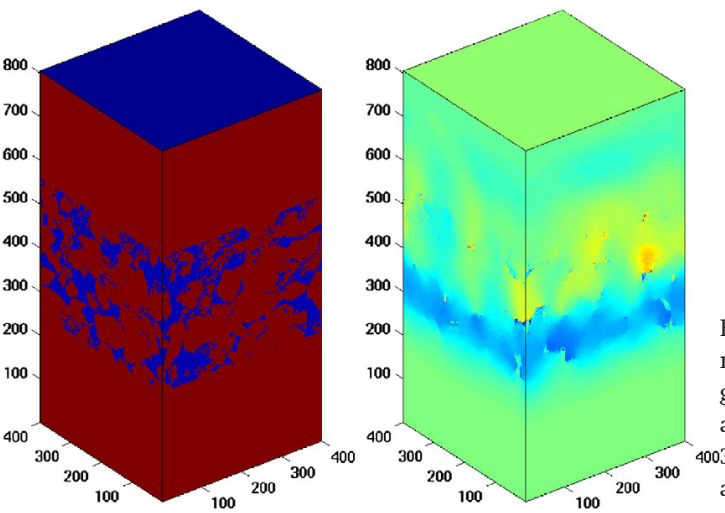

Figure 2. Left hand side: A digital rock with a homogeneous embedding. Red color and blue color indicate grain material and pores, respectively. The used units are grid points (1 [gp]=2.275µm). Right hand side: The 3D vertical displacement field of a plane P-wave generated at the top of the model after several timesteps.

REFERENCES

Saenger E.H., Enzmann F., Keehm Y. and Steeb H., 2011: Digital rock physics: Effect of fluid viscosity on effective elastic properties, Journal of Applied Geophysics 74, 236–241.

21.8

The long-term seismic cycle at subduction thrusts: benchmarking geodynamic numerical simulations and analogue models

Ylona van Dinther[1], Taras Gerya[1], Fabio Corbi[2], Francesca Funiciello[2], P. Martin Mai[3], and Luis Dalguer[1]

[1] Institute of Geophysics, ETH Zurich, Sonneggstrasse 5, CH-8092 Zurich
[2] Department of Geology, Universita degli Studi 'Roma Tre', Roma, Italy
[3] Division of Physical Sciences & Engineering, KAUST, Thuwal, Saudi Arabia

The physics governing the long-term seismic cycle in subduction zones remains elusive, largely due to its spatial inaccessibility, complex tectonic and geometric setting, and the short observational time span. To improve our understanding of the physics governing this seismic cycle, we benchmark a geodynamic numerical approach with a novel laboratory model. In this work we quantify and compare periodicity and source parameters of slip events (earth-quakes and gel-quakes) as a function of fault rheology (i.e. frictional properties).

Our fluid-dynamic numerical method involves a plane-strain finite-difference scheme with marker-in-cell technique to solve the conservation of momentum, mass, and energy for a visco-elasto-plastic rheology. The simulated gelatin laboratory setup constitutes a triangular, visco-elastic crustal wedge on top of a straight subducting slab that includes a velocity-weakening seismogenic zone.

Numerical and analogue results show a regular and roughly comparable periodicity of short, rapid wedge velocity reversals. Ruptures nucleating mainly around the bottom of the seismogenic zone, and propagating upward, cause a distinct and rapid drop in stress within the wedge. To mimic the short duration, high speed and regularity of the analogue results, the numerical method requires a form of steady-state velocity-weakening friction for acceleration, and healing. The necessity of including a variable state component into the numerical simulations is subject of ongoing work. Finally, we extend this analysis by observing the role of different friction laws in large-scale, geometrically more realistic models.

P 21.1

Accurate gravity data correction and 3D gravity forward modeling

Abdelfettah Yassine[1] & Schill Eva

[1] *University of Neuchâtel, Emile-Argand 11, 2000 Neuchâtel, Switzerland (yassine.abdelfettah@unine.ch)*

The correction of topographic effects on gravity data has been simplified in the past by introducing stepwise approximations to the far-field effect, for example, using the Hammer reticular method. This method computes the topography effect using the approximation of this on the gravity stations which came from the topography interpolation. This approximation causes the lost of the resolution especially at and near the gravity station.

In the present study, we propose a new and accurate gravity data correction approach. The area around the measurement point is subdivided into four zones with increasing radiuses: the inner zone, the near zone, the intermediate and the remote zones. Each zone has a specific weight following its distance to the observed gravity station. The accuracy of the calculation is increasing with decreasing distance. Our approach is based on the fact that any topography area can be described by Digital Elevation Model (DEM). Thus from any DEM, we can recover and construct the numerical topography which can be handled by a PC computer in a reasonable calculation time. From the DEM, we construct discrete prisms for which their gravity contribution to the measurement station is calculated. This calculation is carried out for all prisms until total gravity effect of the topography on the gravity station is assessed.

In order to increase accuracy of the topography effect on the gravity station and at the same time reduce computing time, two DEMs with different resolutions are used. The high resolution DEM is used in the inner zone. Sensitivity analyses have revealed the following recommendations to obtain optimum accuracy:

1. It is recommended to take the cell size resolution of the DEM < 5 m and to extend the inner zone up to 150 m from the gravity stations. The gravity effect is computed using the exact formula for a known prism. This prism has a parallelepiped rectangle form.
2. A DEM of lower resolution can be used for the three outer zones. It is first used in the near zone where the prism effect is computed again with the exact formula. Acceptable results is obtained with fixing the 2nd radius at 8 km, but to improve the accuracy, it is recommended to fix it at a distance more or equal to 20 km especially if there are not computing time constraint.
3. The 3rd sub-area is the intermediate zone which is delimited by the near zone and the 3rd radius. Here the DEM of lower resolution is used to assess the gravity effect of each prism by the theoretical basic formula where the gravity effect is concentrated in the center of the prism. This zone can be extended from 8 to 50 km.
4. The last subarea is the remote zone. It is delimited by the intermediate zone and the 4th radius. The DEM of lower resolution is used to generate a new DEM with cell size about 1 x 1km. The altitude of these blocs is the average of all prisms located in the 1 x1 km area. The gravity effect is assessed by the same approach as in the intermediate zone. This area can be extended from 40 to 167km.

Specific considerations are taken an account between the intersection of these four zones especially between the inner and the near zones where the cell size resolution is not equal.

The following parameters can be chosen for the topographic correction: The radius which delimits the four zones, the densities will be use in the topography correction, if one or two DEM will be use, the format of these DEMs (xyz or ISRI), the input files, ...

Forward modeling of the gravity effect in particular for complex 3D geology is based on the same principal described above. Here the current input files are 3D geological models from 3D Geomodeller and Gocad. A selection of output forms, the different layers and their densities for a geological model can be chosen.

The code was tested and validated successfully on the real data for both gravity data correction and forward modeling. An example for the complete Bouguer anomaly obtained by the purposes is showed in Figure 1.

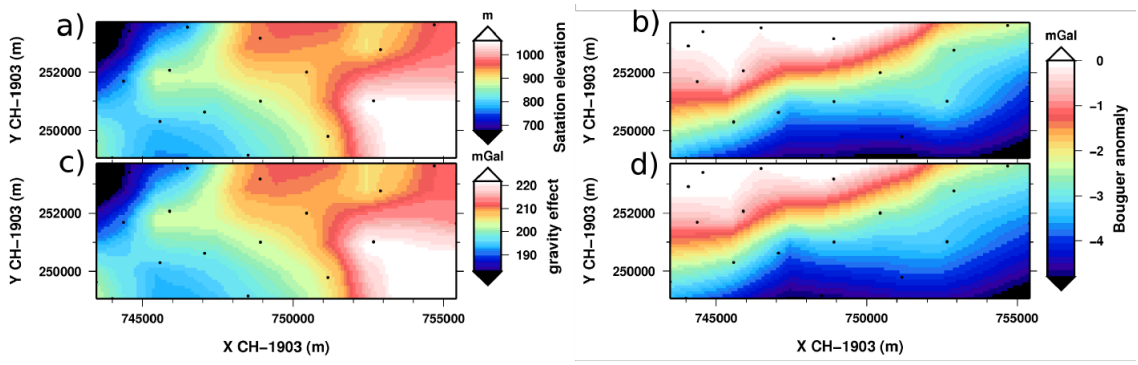

Figure 1: The results of the gravity data processing with a) the gravity station elevations denoted by the black points, b) Bouguer anomaly map computed by the SwissTopo using Hammer reticular method to achieve the topography data correction, c) terrain and the topography effects obtained assuming homogeneous density of 2.67 g/cm³. The gravity stations are located at the real elevation on the topography surface as showed in a). The gravity effect of the area is well recovered and as we can identify it is the Free Air anomaly for the homogeneous model. d) Bouguer anomaly obtained by our method. These results were obtained using 2 DEMs. The 1st used in the inner zone has cell size resolution of 2 m and the 2nd of 25 m. The inner zone is limited by 150 m radius and the near zone is limited by 50 km from the stations. The intermediate zone is bordered by the 3rd radius fixed at 70 km and the remote zone is bordered by 170 km radius.

P 21.2

Characterization of the Upper Muschelkalk aquifer in northeast Switzerland using laboratory physical properties and imaging techniques

Almqvist Bjarne S.G.[1], Aschwanden Lukas[2], Diamond Larryn[2], Ramseyer Karl[2], Zappone Alba[3]

[1]*ETH Zurich, Institute of Geological Sciences, Sonneggstrasse 5, CH-8092 Zurich (bjarne.almqvist@erdw.ethz.ch)*
[2]*University of Bern, Institute of Geological Sciences, Baltzerstrasse 1+3, CH-3012 Bern*
[3]*ETH Zurich, Institute of Geophysics, Sonneggstrasse 5, CH-8092 Zurich*

Deeply buried levels of the Triassic Trigodonus Dolomite Formation of the Upper Muschelkalk aquifer (Swiss Molasse Basin) show potential for geothermal energy exploitation and for geological storage of gas – whether permanent storage of waste CO_2 (Chevalier et al., 2010) or seasonal storage of imported methane. All of these potential applications rely on high porosities and high permeabilities. Although some borehole intersections of the Formation look encouraging, very little is known about the regional distribution and magnitudes of porosity and permeability within the aquifer. In this context we are undertaking a quantitative and qualitative characterization of the porosity and permeability of the Trigonodus Dolomite using a variety of analytical techniques, including SEM imaging, He-pycnometry, mercury porosimetry, thin-section petrography, x-ray computer tomography (CT), as well as ultrasonic velocity and permeability measurements. These laboratory analyses will be integrated with field scale geophysical observations and laboratory geochemical and isotopic investigations.

The porosity of the Trigodonus Dolomite is mainly controlled by prevalent secondary dissolution of cm-scale anhydrite nodules and macrofossils as well as microporosity related to the dolomitization process. SEM imaging shows that large dissolution pores are often connected by inter-grain microporosity (Figure 1a). Additional macropore connectivity is provided by cm to dm long subvertical cracks, as is indicated by coarse resolution CT imaging and visual inspection of the drill core (Figure 1b). The timing of the dissolution of anhydrite nodules and formation of macroporosity is not well known and ongoing isotopic and fluid inclusion studies are aimed at pinpointing the dissolution event within the known temperature–burial depth history of the Formation.

The laboratory porosity measurements, on 2.54 cm diameter and ~3.5 cm length cores from the Benken drill core (Nagra, 2001), range from 8 to 25%. Ultrasonic P wave velocities, measured at ambient temperature and pressure conditions, vary from 3100 to 5800 m/s. The S wave velocities of the corresponding cores are between 1800 and 3500 m/s. In general there

is an inverse relationship between velocity and porosity, although a few samples do not follow this trend. Ongoing permeability measurements will help shed light on the micropore connectivity and hence on the injectivity of gas into storage space. However, the total permeability of the aquifer is likely determined by the subvertical sets of fractures, which are usually missed by drillcore-scale sampling. So far, the laboratory results show a good correlation with borehole geophysical data. This opens the way to calibrate the geophysical signals in order to derive a regionally extensive estimate of porosity and permeability.

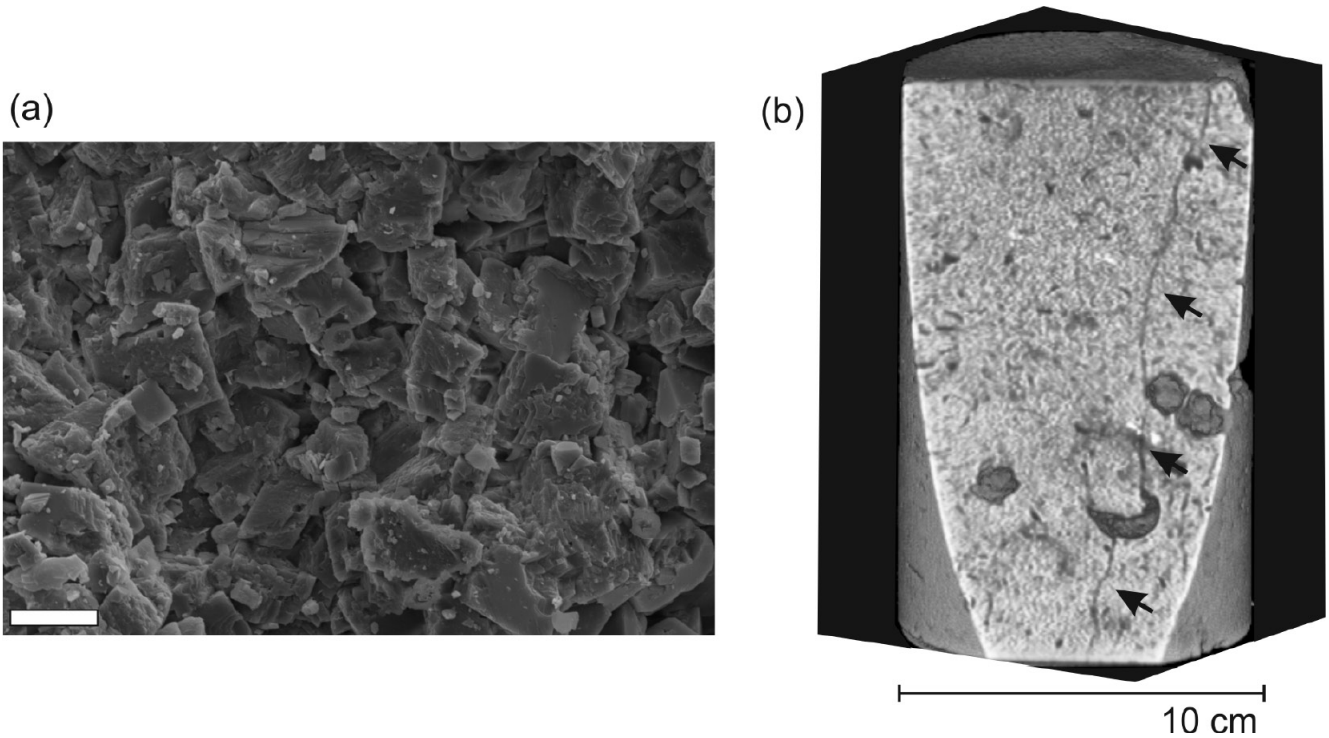

Figure 1. Different imaging techniques used to characterize the Trigodonus Dolomite (Benken, Nagra). (a) SEM image (secondary electron mode) illustrating the dolomite matrix grains and inter-grain porosity, at 825 m below surface (mbs); the scale bar is 20 µm (lower left). (b) A reconstructed CT-image from a core-segment at 827 mbs. A crack longer than 10 cm, with subvertical orientation, is outlined by the arrows. The x-ray tomography was performed at the Universitätspital in Zurich. Processing of the raw data and plotting was done using ImageJ, with the volume viewer 1.31 plugin.

REFERENCES

Chevalier, G., Diamond, L. W. & Leu, W., 2010: Potential for deep geological sequestration of CO2 in Switzerland: a first appraisal. Swiss Journal of Geosciences 103 (3), 427-455.

Nagra, 2001: Sondierbohrung Benken - Untersuchungsbericht. Technischer Bericht 00-01 (288 pp). Wettingen - Nagra.

P 21.3

Toward source characterization of local supershear ruptures in dip-slip faults

Cyrill Baumann[1], Luis Angel Dalguer[1]

The speed at which a rupture propagates is an important factor that contributes to determine the character of the ground motion. Rupture speeds are bounded at the upper end by the maximum speed at which stresses are transmitted through the rock. Most earthquake ruptures propagate with velocities slower than the S-wave speed, while studies of some earthquake data, lab and theoretical physical models reveal the occurrence of rupture velocities exceeding the S-wave speed, i.e. supershear. Most of the attention of those studies has been given to large strike slip fault, because earthquakes in long faults predominantly ruptures in mode II, in which super-shear rupture speed is most likely to occur (see for instance Dalguer et al in this session)

Little attention has been given to evaluate the possibility and importance of the occurrence of supershear speed in dip-slip faults. Though rupture along the length of dipping faults predominantly rupture in mode III, there is also a portion of the rupture that propagate along the dip (mode II direction) in which supershear rupture speed may take place. Here we evaluate this possibility and quantitatively characterize the areas of supershear rupture speed in dip-slip faults. For such as purpose we develop suite of earthquake source physics-based dynamic rupture models. Stress distribution prior to earthquakes was assumed to be stochastic with heterogeneous stress consistent, in a statistical sense, with past earthquakes. We performed series of numerical simulations in 45° dipping normal faults with fault area between 30x20 Km, and 200x28 Km. The resulting earthquakes cover a range magnitude Mw = 5.29-7.89.

Our dynamic rupture simulations reveal that in rupture propagating along heterogeneities stress fields, the stress waves ahead of the rupture front encounter patches of pre-stress close to the yielding criteria. If these waves have sufficient amplitude, they can trigger short-lived periods of secondary rupture that can trigger localized supershear propagation. In the current simulations, this localized area is limited to areas along the width of the fault at the hypocenter zone, and increases with the earthquake size. For magnitude in the range 6.3 <= Mw <= 7.5 this area increase respectively from 1% to 10% of the total rupture area.

Our final goal is to identify signatures of this localized supershear rupture speed on seismograms to assess the level and variability of ground motion in a certain areas for seismic hazard and risk mitigation.

P 21.4

Laboratory simulations of tensile (hydro) fracture: current work and new directions

Benson, Philip[1], Heap, Michael[2], Lavallée, Yan[3], Flaws, Asher[3], Hess, Kai[3], Cordonnier, Benoit[1] and Misra, Santanu[1]

[1] *Geological Institute, Swiss Federal Institute of Technology, Zurich, Switzerland (philip.benson@erdw.ethz.ch)*
[2] *École et Observatoire des Sciences de la Terre, Strasbourg, France*
[3] *Geo- und Umweltwissenschaften, LMU, Munich, Germany*

During magma ascent, cracking and faulting of the host rock provide conduits for the movement of magmatic fluids. The spatial and temporal formation of such conduits, driven largely by pressurized magmas in the form of dykes, is of key importance in the volcano-tectonic system. In particular, it is known that both a fracture mechanical (brittle) mechanism (due to the propagating dyke tip) as well as a petrological mechanism (due to the elevated pressure-temperature environment), play roles in dyke propagation. As the use of elevated temperatures in the laboratory is technically challenging, early work has tended to concentrate either on analogue setups using gelatine and other materials that are fractured by injection of coloured water (Menand and Tait, 2001; Acocella et al., 2001; Walter and Troll, 2003), or – for simulation of representative pressures – a simplified setup at modest (room) temperatures. In this latter case, a relatively simple (room temperature) cylindrical setup is feasible using water as a pressurising fluid and with an axial conduit lined with a rubber membrane to isolate the fluid from the rock matrix (e.g. Vinciguerra et al., 2004).

Here, we overcome these difficulties by simulating magma intrusion in the laboratory through an experimental protocol that compresses a 'conduit' of magma encapsulated inside a hollow shell. A well-controlled stress is then imposed onto the conduit which has the effect of transmitting this force onto the inner wall of the surrounding shell. Although we present our work with a view to investigating fluid driven tensile fracture applicable to high temperature processes, this general protocol may be used to analyse a wide range of processes whereby direct fluid pressure is used to fracture a host medium. Common examples include hydrofracture in engineering geology applications (gas shale) as well as in engineered geothermal systems for the creation of injection and production water/steam wells. To analyse the system, we use a suite of well-known fracture mechanics methods allied to independently measured rheological parameters for the conduit to develop a model to explain (a) the stress relaxations, and (b) the peak stress measured at failure, as well as the observed interactions between the ductile inner conduit and brittle outer shell, interpreted as analogous to dykes driving though a volcanic edifice.

We conclude that (a), the coupling of stress, strain and seismic data through time can be used to infer the stability of volcanic conduits and/or the state of the magma during periods of unrest by calculating the viscoelastic relaxation parameters and hence the modulus or viscosity of the melt, (b), dyke propagation is initiated when the tensile strength of the country rock is overcome, between 7-11 MPa, in the case of basalt from Etna Volcano, and that the initial tensile failure is energetic enough to melt, and to produce shock waves in it, (c), that the fracture of silicate melt is strain rate dependent (Dingwell and Webb, 1989) and (d), that the material fracture parameters are largely temperature independent. Future plans in the rock deformation laboratory at ETH Zurich (Fig. 2) aim to extend this approach to elevated temperatures **and** confining pressures in order to simulate processes at depth.

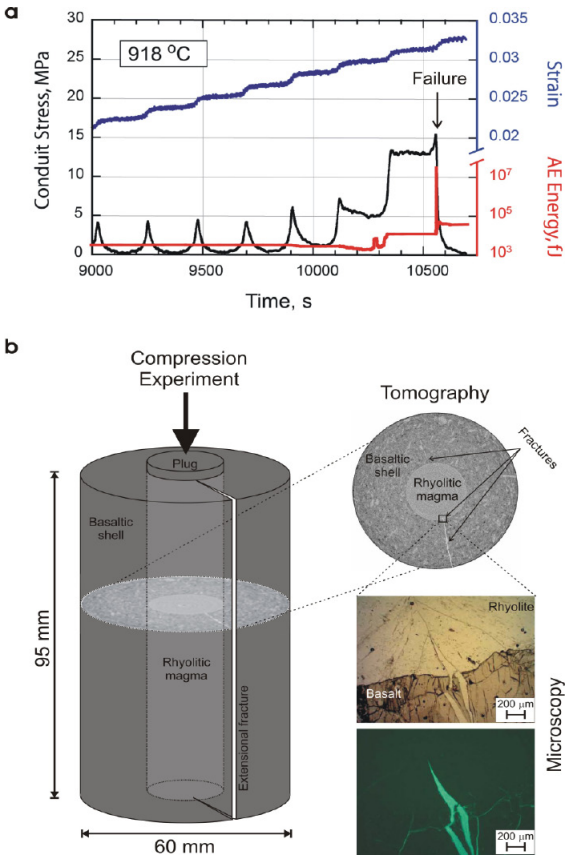

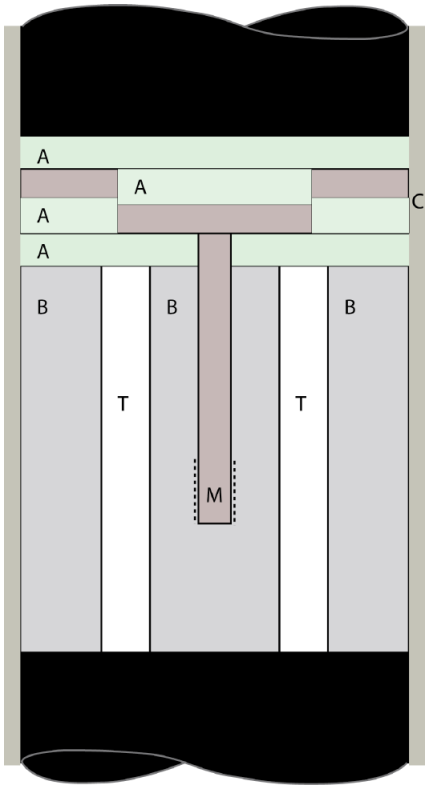

Fig. 1 (left). Magma/conduit interaction experiments. The application of pressure onto a solid basaltic plug compressed a rhyolitic magma (light grey) against the solid inner shell of basalt (dark grey). Fig. 2 (right): Concept of future experiments to add a confining pressure to the system via a Paterson type gas medium apparatus [A: Alumina spacers/piston; B: basalt; M: Melt, for internal pressurisation; T: Welded Tuff; C: Copper jacket].

REFERENCES

Acocella, V., F. Cifelli, R. Funiciello (2001), The control of overburden thickness on resurgent domes: insights from analogue models, J. Volcanol. Geotherm. Res., 111, 137-153.

Dingwell, D.B., Webb, S.L. (1989), Structural relaxation in silicate melts and non-Newtonian melt rheology in geologic processes. Phys. Chem. Miner., 16 (5), 508–516.

Menand, T., and S. R. Tait, (2001), A phenomenological model for precursor volcanic eruptions. Nature, 411, 678-680.

Vinciguerra, S., P. G. Meredith, and J. Hazzard (2004), Experimental and modelling study of fluid pressure-driven fractures in Darley Dale sandstone, Geophys. Res. Lett., 31, L09609, doi:10.1029/2004GL019638.

P 21.5

Physical mechanisms for low-frequency seismic wave attenuation in fractured media

Marcel Frehner[1] & Beatriz Quintal[1]

[1]*The Rock Physics Network at ETH Zurich (ROCKETH), Sonneggstrasse 5, CH-8092 Zurich (marcel.frehner@erdw.ethz.ch, beatriz.quintal@erdw.ethz.ch)*

Attenuation and dispersion of seismic waves is an important parameter for analyzing seismic data, because it can provide additional information compared to analysis based only on velocity and density. Understanding the mechanisms causing attenuation is a challenging rock physics task. We present two physical mechanisms that can cause attenuation and dispersion of seismic waves.

1. Wave-induced fluid flow
2. Krauklis wave initiation

Both mechanisms are studied numerically using the finite-element method.

1. Wave-induced fluid flow

We performed numerical simulations of a quasi-static experiment to calculate attenuation (1/*Q*) caused by wave-induced fluid flow in a heterogeneous poro-elastic medium (with patchy saturation and double porosity). The methodology is described in Quintal et al. (2011) and COMSOL Multiphysics was used for these simulations. The finite element method using an unstructured mesh (Figure 1) was applied. The model consists of gas-saturated kerogen-rich shale with open fractures, which are saturated with water (injected during the fracturing). The fractures, also shown in Figure 1, are 4, 3, and 5 mm thick, respectively, from left to right. The medium is considered to be a repetition of the Representative Elementary Volume (REV) shown in Figure 1.

The results of the simulation are shown in Figure 2. The minimum value of *Q* is 10.2 at 1.6 Hz. *H* is the P-wave modulus, such that $V_P = \sqrt{H/\rho}$. From the simulation with closed calcite fractures, *Q* = infinite (and constant), and Re(*H*) = 2.5 GPa (constant).

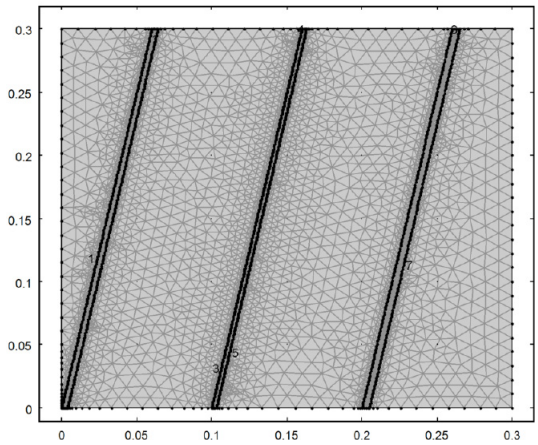

Figure 1: Model (0.3 x 0.3 m) and the unstructured triangular finite-element mesh of the fractured medium.

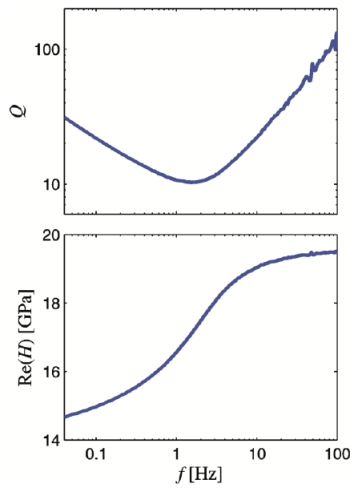

Figure 2: Results for the quality factor (*Q*) and the real part of the P-wave modulus (*H*).

2. Krauklis wave initiation

The Krauklis wave is a special wave mode that is bound to and propagates along fluid-filled fractures and can also influence seismic body waves. Krauklis waves can propagate back and forth along a fracture and emit a periodic signal (Frehner and Schmalholz, 2010). Seismic data can contain this characteristic frequency and eventually reveal fracture-related petrophysical parameters of the reservoir. Krauklis waves are well described mathematically for some theoretical cases. However, one key question that is still unclear is how Krauklis waves are initiated by a body wave passing a fluid-filled crack. Figure 3 shows a finite-element study for the case of a plane P-wave passing an elliptical water-filled crack with 45°

inclination. The P-wave is scattered and diffracted at the crack and two Krauklis waves are initiated, one at each crack tip (i.e., diffraction points). For more realistic crack geometries and/or intersecting cracks, more diffraction-points will lead to a higher probability to initiate Krauklis waves.

The initiation of Krauklis waves by a passing body wave represents an energy transfer from the body wave to the fracture, and therefore an attenuation mechanism for the body wave. By propagating back and forth the fracture, the Krauklis wave can emit a periodic body wave signal (Frehner and Schmalholz, 2010), which leads to a strong dispersion of the body wave. The efficiency of these processes remain to be studied in the future.

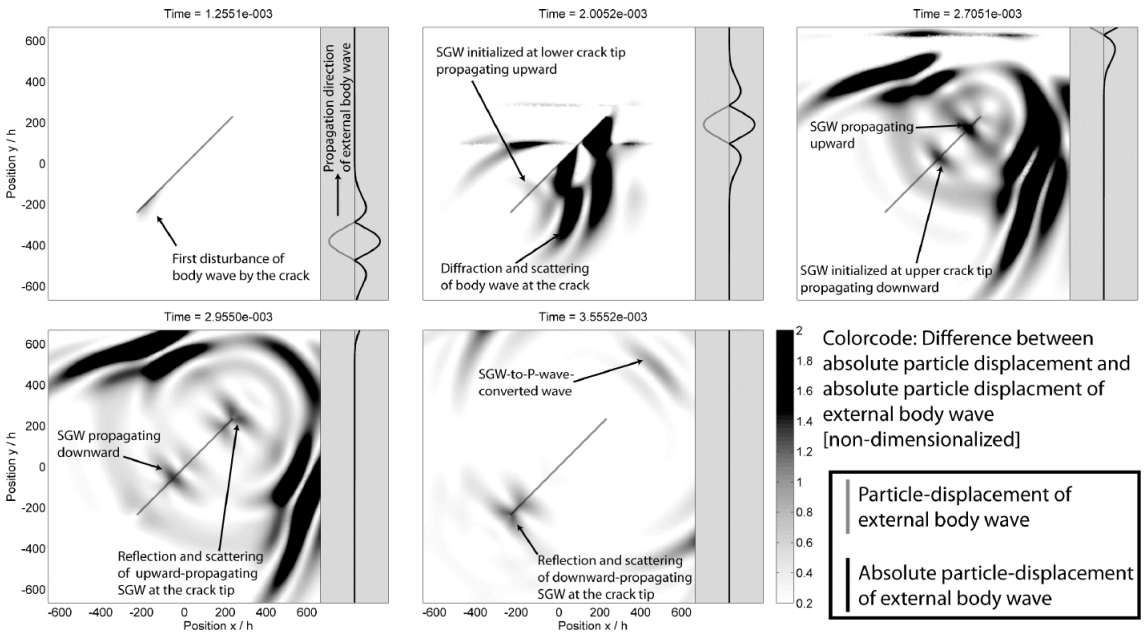

Figure 3: Snapshots of Krauklis waves being initiated by a passing plane P-wave. The single wavelet P-wave propagates from bottom to top and its profile is shown in the gray sidebars. The signal of the passing P-wave is subtracted from the total absolute particle displacement for better visibility.

REFERENCES

Frehner, M. and Schmalholz, S.M., 2010: Finite-element simulations of Stoneley guided-wave reflection and scattering at the tips of fluid-filled fractures, Geophysics 75, T23–T36.

Quintal, B., Steeb, H., Frehner, M. and Schmalholz, S.M., 2011: Quasi-static finite element modeling of seismic attenuation and dispersion due to wave-induced fluid flow in poroelastic media, Journal of Geophysical Research – Solid Earth 116, B01201.

P 21.6

Rock classification based on physico-mechanical analysis -case study: Poshtkuh basin, Alborze region-Iran

Kaveh Khaksar[1], Marahem Rahmati[2]

[1]*Institute of Scientific Applied Higher Education of Jihad-e-Agriculture, Dep. of Soil Science, Education and Extension Organization, Ministry of Agriculture, Iran. Email: kavehkhaksar@gmail.com*
[2] *Expert of Fishery Research Center, Tehran-Iran*

This paper is derived from a research on rock classification using geological hammer, Schmitt hammer, fissure and joints, in the Maharlu basin in southwest of Iran.
The mechanical breaking and dissecting of rocks occurs in the regions, which the changes of temperature and humidity are considerable. The weathering of the geological formations depends on different factors, which have divided in two groups: 1) Superficial factors such as climatic conditions, topography, vegetation covering and human weathering system and 2) Bed rock and its physical and chemical characters.

Poshtkuh basin is located in Semnan province. The Middle Triassic and the Quaternary units are respectively the oldest and youngest rocks in the basin. Since the studied area is generally composed of sedimentary rocks and sediments like marl, shale, marly shale, conglomerate, sandstone and limestone rather have spread. The region is mainly composed of sedimentary deposits. The Poshtkuh basin lies in the North of Iran (Alborz range) and mainly calcareous rocks crop out in this area. It were carried out three physical and mechanical analyses to evaluate the sensitivity of rock units to weathering. The fissure and joints were measured, evaluation of mechanical properties and grade of weathering were also measured by using a Schmidt hammer and rock resistance was estimated by geological hammer. The acquired data from the various rock types constituting the basin were analyzed, and their sensitivity to weathering was determined. Finally, a map of erosion sensitivity was prepared for different geological units. In the base of the acquired results, the geological units of poshtkuh basin respect to erosion have been classified to:

Low: Member Jkl^3, Upper part of Lar Formation J_1^2, Tizkuh Formation k_t, Member k_1^1, Member $k_1^{s.1}$, Member k_2^1, Ziarat Formation (Pe_z), Member J_1^1
Low to medium: Elika Formation TRe3, Unit J_S^{le}, unit $k_2^{t,l}$
Medium: Member $J_{S,}$ Member k_2^v, Member $k_1^{l,m}$, Fajan Formation (pg_f^c), Karaj Formation (E^K), Member J_S^4
Medium to great: Member J_S^3, Member $E^{l,sh}$
Great: Shemshak Formation TR3js, unit TR3JS1, unit J_S^2, Delichai Formation, unit (J_D), unit (E^{sh}), Quaternery deposites.
Finally the map of different geological unit resistivity to weathering of Poshtkuh basin has been assigned.

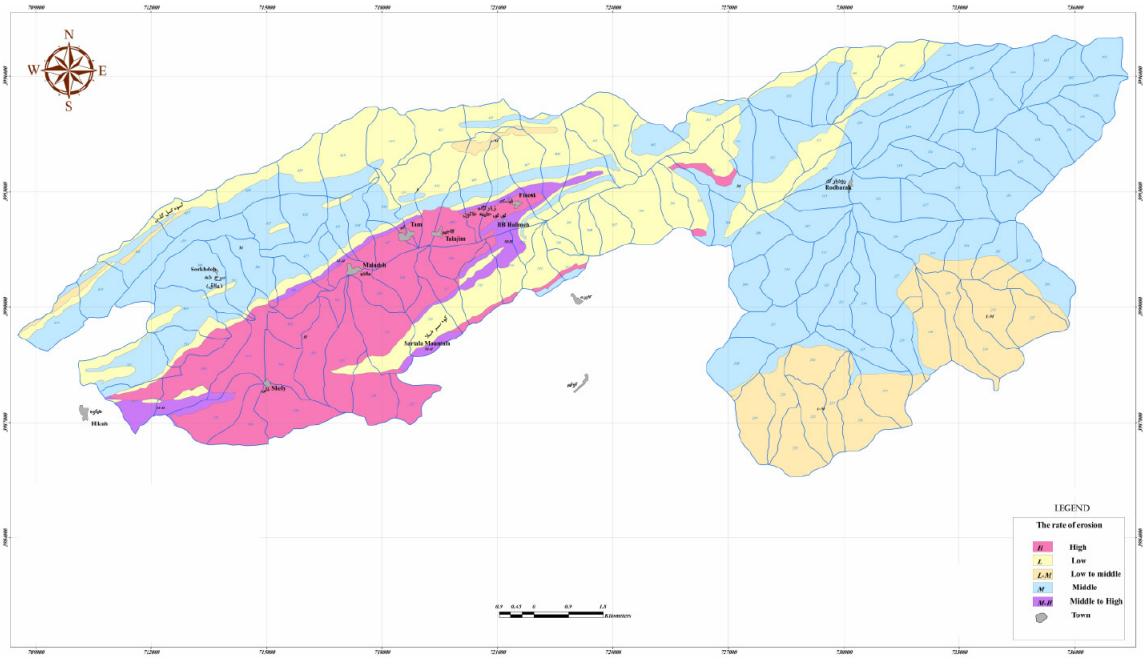

Figure. 1 Map of rock classification in the Poshtkuh Basin

REFERENCES

Arzani, N. (2006) Primary versus diagenetic bedding in the limestonr-marl/shale alternations of the eperic seas, an example from the lower Lias (Early Jurassic) of SW Britain, V. 21, N. 1, 94-109.

Bieniawski, Z. T. (1989) Engineering rock mass classifications. Chichester, Wiley.

Garnett, C. S. (2009) On a Local Alteration in Limestone Shales at Wensley, Derbyshire, Geological Magazine (1921), 58: 473-477.

Gomez, F. P. (1995) Erosion E Inestabilidad en la Cuenca del Rio Patana (Alpujarra alta Almeriense), Instituto de Estudios Almerienses. Pp. 74.

Hunt, R. E. (1984) Geotechnical Engineering Investigation Manual, Mc Graw Hill, 896 P.

ISRM (1979) Suggested methods for determining in situ deformability of rock," ISRM Commission on Standardization of Laboratory and field Tests, Int. J. Rock Mech. Min. Sci. Geomech. Abstr., 16(3), 195-214.

ISRM (1981a) Basic Geotechnical Description of rock masses, Int. J. Rock Mec. & Min. Sci.; Vol, 18, N 1. Pp. 85-110.

Kent, P. E. (2009) The Limestone-Shale Rhythm in the British Lower Lias, Geological Magazine (1957), 94: 429-430.

Khaksar & Roozkhash (2007) Evaluation sensitivity classification of rock units and unconsolidated deposits to erosion, 6th International symposium on Mediterranean Geology, April 2-5, 2007, Amman-Jordan.

Khaksar, Goodarzi, Rahmati, Gharibreza (2006) Sensitivity determination of geological formations, Maharlu basin, Quarterly of Geological Science, No: 62.

P 21.7

Low frequency measurements of seismic wave attenuation

Madonna Claudio [1], Tisato Nicola [1] and Saenger Erik H. [1]

[1]*Geologisches Institut, Sonneggstrasse 5, CH-8092 Zürich (claudio.madonna@erdw.ethz.ch)*

The study of wave attenuation in partially saturated porous rocks over a broad frequency range provides valuable information about reservoir fluid systems, which are inherently composed of multiple phase fluids. The main goal of our work is to experimentally measure the bulk attenuation on partially saturated rocks at frequencies between 0.01 and 100 Hz, using natural rock samples under in situ conditions. To fulfil this aim, we designed and set up a specific instrument: the Seismic Wave Attenuation Module (SWAM). We present its bench-top calibration, a series of data collected from different kind of rocks and the numerical simulations, which support the obtained results.
We employ the sub-resonance test. Assuming that the rock behaves as a linear time invariant (LTI) system, the attenuation factor Q^{-1} (Q is the quality factor) is equal to the tangent of the phase shift between the stress and the strain signal. This also corresponds to the ratio between the imaginary and the real part of the transfer function (Nowick and Berry; 1972, Jackson and Paterson, 1987). The phase lag (θ) is calculated by the difference obtained using the Fourier transform between phases of the stress and strain signals. Equation 10 of O'Connolly and Budiansky (1978) shows the relation between attenuation Q^{-1} and the parameter gathered from the experiments can be expressed:

$$Q^{-1} = \frac{\Delta E}{2pE} = \tan|q|$$

The phase lag, θ, can be seen as the ratio of the energy loss ΔE and total energy E introduced into the rock for each cycles.

Figure 1 is a sketch of the operating systems. To obtain precise and accurate measurements over a wide range of experimental conditions the SWAM apparatus measures, in an automated way, the bulk attenuation of non-homogeneous and partially saturated samples. Each sample is 60 mm long and 25.4 mm in diameter.

Our system makes a bulk attenuation measure across the whole sample length in contrast to the measurements using strain guages. This is accomplished by measuring the strain across the whole sample with micro-linear variable differential transformers (micro-LVDT). This technique allows acquiring many values from all kinds of rocks: from consolidated granular materials up to highly dense and compact rocks. The magnitude of finite strain is in the order of 10^{-6} .

The device is comprised of two main elements: (1) A piezo-electric stack actuator (PZ) generates dynamic displacement. A sinusoidal axial compressive stress is applied by the relative vertical displacement of the PZ-actuator. The actual oscillating frequency ranges from 10^{-2} to 10^{2} Hz with amplitudes from nanometers to micrometers. (2) Two displacement measurement modules consist of micro-LVDT's. These transformers measure the compression and extension strains of both the sample and a purely elastic standard with a nanometric resolution. The strain across the purely elastic standard is the reference signal to which we compare the strain across the sample for any phase lag induced by anelasticity.

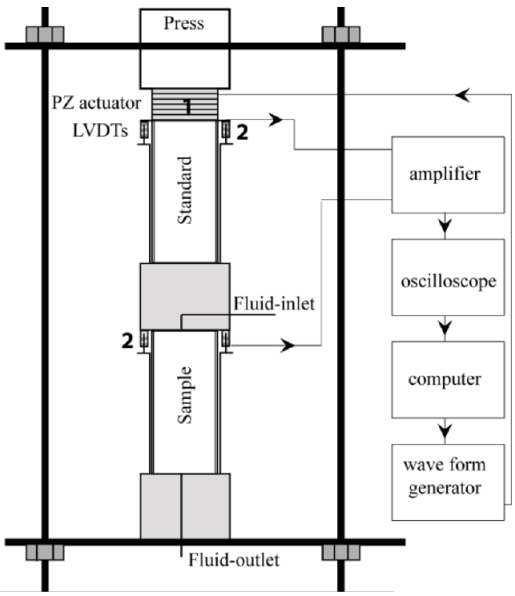

Machine characteristics	
Name	S.W.A.M
Frequency range	0.01-100 Hz
Sample length	60-100 mm
Sample diameter	25.4 mm
Sensors	LVDT
Planned confining pressure	200 MPa

Figure 1. The stress is applied employing a piezo-electric actuator (1). Shortening of both the elastic element and the sample is measured through LVDTs (2).

REFERENCES
Jackson, I., and M. S. Paterson, [1987] Shear modulus and internal friction of calcite rocks at seismic frequencies: pressure, frequency and grain-size dependence. Phys. Earth Plan. Int., 45, 349-367.
Nowick, A. S., and Berry, B. S. [1972], Anelastic relaxation in crystalline solids: Academic Press, New York.
O'Connell and Budiansky [1978], Measures of dissipation in viscoelastic media, Geophys. Res. Lett., 5(1), 5-8.

P 21.8 *(see P 20.4)*

Changes of Coulomb Failure Stress due to Dislocations during Stimulation of GPK2 at Soultz-sous-Forêts

Schoenball, Martin[1,2], Baujard, Clément[1], Kohl, Thomas[1,2] & Dorbath, Louis[3]

[1]*GEOWATT AG, Dohlenweg 28, CH-8050 Zürich (schoenball@geowatt.ch)*
[2]*Karlsruher Institut für Technologie, Institut für Angewandte Geowissenschaften, Kaiserstr. 12, D-76131 Karlsruhe*
[3] *EOST, University Louis Pasteur, 5, rue René Descartes, F-67084 Strasbourg*

The European deep geothermal research project at Soultz-sous-Forêts (Alsace, France) has been developed since 1987. The geothermal reservoir is situated in a horst structure within the granite basement of the Upper Rhine Graben. During the project for developing an Enhanced Geothermal System (EGS) several well stimulations have been conducted and induced several tens of thousands of microseismic events. During the stimulation of well GPK2 the maximum event recorded during stimulation reached magnitude 2.5.
In the field of seismology of tectonic earthquakes, aftershock sequences produced by a large magnitude main shock have been successfully described by changes of Coulomb failure stress due to the dislocation (in the following denoted as ΔCFS) by the main shock (e.g. King et al. 1994 and Toda et al. 2003).

We present 3D computations of ΔCFS by different geometries of the fault plane to find a computationally efficient way to approximate circular sources taking into account an appropriate slip distribution. We then compute transient ΔCFS in the Soultz reservoir during the stimulation of GPK2. For this analysis we use an extensive database of over 700 derived focal mechanisms (Dorbath et al. 2009). This allows us to conclude that the stress perturbation of all microseismic events during stimulation cannot be depicted by one single fault. Furthermore analysis of this dataset allows us to estimate the influence of ΔCFS by dislocation over the total change of Coulomb failure stress by other processes like the increase of pore fluid pressure, thermal stresses, hydraulic response of the reservoir and coupling of these.

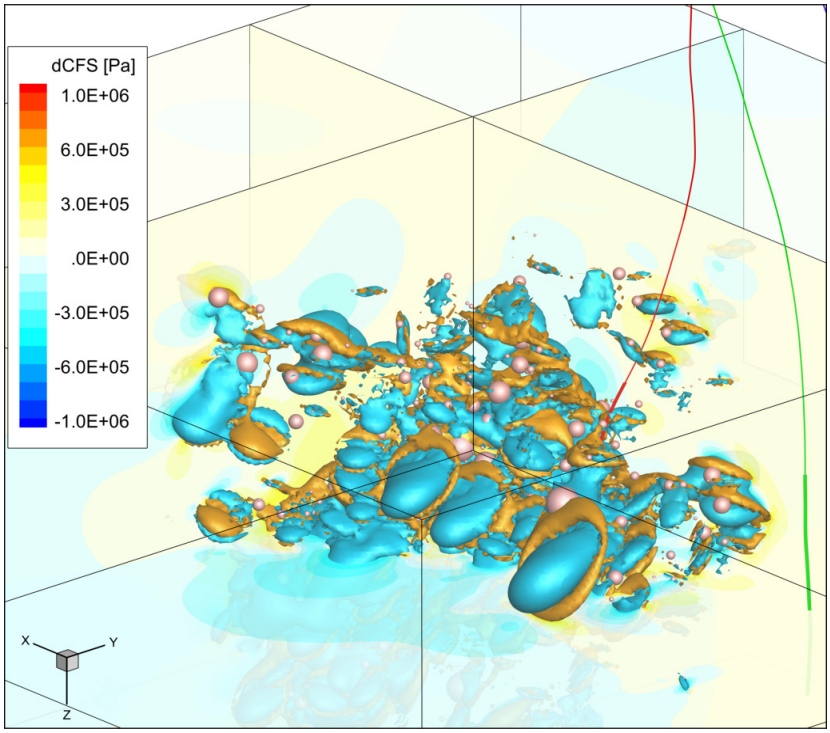

Figure 1. 3D views of ΔCFS in the Soultz reservoir with isosurfaces at ±0.5 MPa. The wells GPK2 (red), and GPK3 (green) are displayed with bold open hole section. The microseismic events used for the computation are represented by sphere symbols that scale with the event magnitude.

REFERENCES

Dorbath, L., Cuenot, N., Genter, A. & Frogneux, M. 2009:. Seismic response of the fractured and faulted granite of Soultz-sous-Forets (France) to 5 km deep massive water injections. Geophysical Journal International, 177(2), 653–75.

King, G. C. P., Stein, R. S. & Lin, J. 1994: Static stress changes and the triggering of earthquakes. Bulletin of the Seismological Society of America, 84(3), 935–953.

Toda, S. & Stein, R. 2003: Toggling of seismicity by the 1997 Kagoshima earthquake couplet: A demonstration of time-dependent stress transfer. J. Geophys. Res., 108(B12), 2567.

P 21.9

Measurements and mechanisms of seismic wave attenuation in partially saturated rocks

Nicola Tisato[1], Claudio Madonna[1] & Erik H. Saenger[1,2]

[1]*ETH Zurich, Soneggstrasse, 5, CH 8092 Zurich (nicola.tisato@erdw.ethz.ch)*
[2]*Spectraseis, Giessereistrasse 5 CH 8005 Zurich*

Seismic wave attenuation of low frequency seismic waves in the earth crust has been explained by partial saturation (Goloshubin, 2006) and permeability models (e.g. Pride et al., 2004). We present the latest results obtained with the Broad Band Attenuation Vessel (BBAV), which measures seismic wave attenuation in the range of 0.1 - 100 Hz under confining pressures up to 25 MPa. In addition, the apparatus can investigate fluid flow through the pore structure (White, 1975), which can explain the attenuation measurements. The description of the BBAV is also reported, B.B.A.V.

The calibration of the mono-frequency attenuation measurements was completed by testing aluminum and a PMMA (Plexiglas) sample. These two materials represent elastic and anelastic end-members, respectively. Calibrations match literature (Nowick and Berry, 1972; Lakes, 2009).

Two 76 mm diameter and 250 mm long Berea sandstone samples, with different permeability, were tested. The first sample (BS001) had 200-500 mD permeability, while the other sample (BS002) had 500-1000 mD permeability; both the specimens were 20% porosity. The stress conditions were: (1) $\sigma1=3.5$ MPa, $\sigma2=\sigma3=0$ MPa (unconfined) and (2) $\sigma1=18.5$ MPa, $\sigma2=\sigma3=15$ MPa (confined), where $\sigma1$ was the vertical stress. For unconfined conditions, dry samples exhibit attenuation values of about 0.01; when they are 90% water saturated the same samples show attenuation values between 0.018 and 0.028 across the frequency range. For confined conditions, the samples exhibit always attenuation values around 0.01.

Five pore pressure sensors are inserted 38 mm deep in the specimen at different heights along the sample length. This allows continuous and local measurements of pore pressure changes generated by stress field changes. This additional capability of BBAV provides important information about the attenuation mechanisms during stress changes (Mavko et al., 2003). When the sample is 0% water saturated, there is no change in the pore pressure. This result is a benchmark that the measurements are not influenced by the deformation of the rock solid frame. When saturation is more than 60% pore pressure starts to be influenced by the stress field changes. Finally, when the rock is 90% water saturated, the increase of pressure is maximum for the two bottom sensors and around 8 mBar.

Attenuation measurements show that attenuation is frequency-dependent when the samples are unconfined. This observation can be explained by squirt flow (Mavko and Jizba, 1991). According to the characteristics of Berea sandstone, squirt flow should be active between 7 and 7000 Hz. On the contrary, the rock cracks could be closed when the samples are confined, impeding attenuation related to this mechanism. Additionally, pore pressure measurements indicate that stress induced fluid flow is active when the rock is more than 60% water saturated and unconfined.

REFERENCES
Goloshubin, G., Van Schuyver, C., Korneev V., Silin, D., and Vingalov, V., 2006: Reservoir imaging using low frequencies of seismic reflections. The Leading Edge, 25, 527–531.
Lakes, R., 2009: Viscoelastic materials, Cambridge University Press, Cambridge; New York.
Mavko, G., Mukerji, T., and Dvorkin, J., 2003: The rock physics handbook. Cambridge University Press,Cambridge.
Mavko, G., and D. Jizba, 1991: Estimating grain-scale fluid effects on velocity dispersion in rocks, Geophysics, 56(12), 1940, doi:10.1190/1.1443005
McKavanagh, B., and Stacey, F. D., 1974: Mechanical hysteresis in rocks at low strain amplitudes and seismic frequencies. Physics of the Earth and Planetary, 8 (3), 246-250.
Nowick, A. S., and Berry, B. S., 1972: Anelastic relaxation in crystalline solids. Academic Press, New York.
Pride, S.R., Berryman, J.G., and Harris, J.M., 2004: Seismic attenuation due to wave-induced flow. J. Geophys. Res., 109, B01201.
White, J. E., 1975: Computed seismic speeds and attenuation in rocks with partial gas saturation. Geophysics, 40, 224-232.

P 21.10

The Swiss Atlas of Physical Properties of Rocks (SAPHYR): Progress and developments

Zappone Alba [1], Bruijn Rolf[2], Tripoli Barbara[2], Biedermann Andrea Regina[3], Burg Jean-Pierre[2] & Kissling Eduard[3]

[1]*Institute for Process Engineering, Sonneggstrasse 3, CH-8092 Zurich (alba.zappone@sed.ethz.ch)*
[2]*Geological instituteETH Zurich, Sonneggstrasse 5, CH-8092 Zurich*
[3] *Institute of Geophysics, ETH Zürich, Sonnegstrasse 5, CH-8092 Zurich*

Since 2006, a multi-year project supported by the Swiss Geophysical Commission (SGPK), aims to digitize all existing data on physical properties of rocks exposed in Switzerland and to place these data in a referenced geographical frame (GIS). The ultimate goal is to make these data accessible to an open public including industrial, engineering, land and resource planning companies as well as academic institutions.

The systematically measured physical properties are density and porosity, seismic, magnetic, thermal properties, permeability and electrical properties. For the time being, data from literature have been collected extensively for seismic and magnetic properties and only partially for the other physical properties.

In the past two years an effort has been placed on collecting samples and measuring the physical properties of the geologic formations that were poorly documented in the literature. The phase of laboratory measurements is still in progress. We present the updated outputs : a map of Switzerland with sample location, a density map, and maps with contoured and color-coded values of seismic Vp and Vs extrapolated to room conditions from the high pressure laboratory measurements (matrix or crack free properties). We expect to publish the first results of this Atlas of Switzerland by the end of 2011 ..

P 21.11

Carma – Carbon Management in Power Generation: Geological CO_2 storage in Switzerland

Zappone Alba[1-4], Diamond Larryn[2], Almqvist Bjarne[3], Evans Keith[3], Deichmann Nicolas[4], Werner Mischa[1] & Mazzotti Marco[1]

[1] *Institute of Process Engineering, ETH Zurich, Sonneggstrasse 3, CH-8092 Zurich (alba.zappone@sed.ethz.ch)*
[2] *Institute of Geological Sciences, University of Bern, Baltzerstrasse 1+3, CH-3012 Bern*
[3] *Geological Institute , ETH Zurich, Sonneggstrasse 5, CH-8092 Zurich*
[4]*Swiss Seismological Survey, ETH Zurich, Sonneggstrasse 5, CH-8092 Zurich*

The CARMA project aims to explore the potential for and the feasibility of the deployment of CCS in Switzerland within the framework of future energy scenarios. Moreover, we aim to exploit the available expertise to develop new CCS technologies and know-how, which might be applied in Switzerland and worldwide. As to the potential role of CCS, we intend to address and to evaluate the economical, environmental, societal, and institutional implications of CCS, as well as to assess the potential CO_2 geological storage capacity in Switzerland. As to the new technologies, we intend to build on the strengths, experience and available equipment of the research groups involved, focusing on the so-called pre-combustion capture, i.e. the production of hydrogen, its separation from CO_2 and its use in a gas turbine for power generation, and on mineral carbonation, as a means of fixing CO_2 in stable, mineral form. The CARMA consortium brings together the research groups at ETH Zurich, EPF Lausanne, FHNW, Paul Scherrer Institute and University of Bern. The project started in January 2009, with a total runtime of 4 years. This poster presentation shall report the achievements with respect to geological storage of CO_2 in Switzerland during the first half of the project.

An estimate of the theoretical storage potential in the subsurface of Switzerland was completed in August, 2010. The methodology followed an existing evaluation scheme developed in Canada, which is based on geological criteria only. Modifications were introduced to suit the geological setting and available data in Switzerland. The study relies on nine quantitative and semi-quantitative attributes derived from analysis of existing drillhole, geological, and geophysical data. The weighted combinations of these attributes have been ranked in order to visualize Switzerland's storage potential in the form of a contour map (resolution = a few km^2). While the entire crystalline body of the Alps plus the southern part of Switzerland lack suitable geological formations for storage, the sedimentary rocks below vast parts of the Central Plateau, in contrast, show moderate to very good potential. The theoretical storage capacity of the suitable sandstone and limestone aquifers is approximately 2.6 Gtons of CO_2, i.e. 65 times Switzerland's current annual CO_2 emissions. Thorough geological investigations and one or multiple field tests would be imperative to prove its feasibility and safety.

Motivated by Switzerland's recent experience with injection-induced seismicity in Basel, the potential seismic hazard related to CCS operations is sought to be carefully assessed within CARMA. In particular, a catalogue of case histories has been compiled documenting the seismic response of the underground to fluid injection in Europe. The compilation includes Enhanced Geothermal Systems (EGS), hydrothermal plants (fault and aquifer utilization), and CCS projects. Data describing each case history includes the type of operation, the depth of the injection, the injection pressure, the net fluid volume injected, the duration and time distribution of the injection activity, the rock type, the tectonic regime and state of stress, and background seismicity of the injection area. Injection at sites with low natural seismicity, defined by the expectation that the local peak ground acceleration from natural earthquakes has less than a 10% chance of exceeding 0.08g in 50 years, has not produced felt events. Although the database is limited, this suggests that low natural seismicity, corresponding to hazard levels below 0.07g, may be a useful indicator of a low propensity for fluid injection to produce felt or damaging events.

An alternative approach to that offered by subsurface storage is ex-situ mineral carbonation in a controlled industrial setting. This involves the dissolution of CO_2 into an aqueous phase, leaching of magnesium/calcium from a natural mineral feedstock and the precipitation of Mg-/Ca-carbonates, thus fixing CO_2 in a stable, environmentally benign form. The reactions involved are exothermic overall, but their kinetics are slow under ambient conditions. This makes an energy intensive mechanical or thermal activation of the mineral feedstock inevitable. While this adds to costs, mineral carbonation offers the possibility of fixing CO_2 directly from an industrial off gas stream, thus obviating the costly capture step. Within the CARMA project, we are investigating an aqueous process, where a flue gas is bubbled through a stirred tank containing the mineral feedstock in suspension. Temperature is kept low to enhance gas solubility and the total pressure will be kept close to ambient to prevent co-pressurization of the non-CO_2 flue gas components. Carbonate precipitation takes place either in the same vessel, or from the filtered, Mg/Ca and CO_2 loaded solution in a second tank. We have built a set-up to perform mineralization experiments under a variety of temperature, pressure, gas composition and solution chemistry conditions, using several optical and physicochemical analytical techniques to monitor the different phases in-situ and online further downstream. Currently, the dissolution behavior of thermally activated serpentine is being studied. Hitherto, olivine was found to be the natural silicate feedstock exhibiting fastest dissolution kinetics. When directly compared to olivine, we found that activated serpentine dissolves 2 to 3 orders of magnitude faster under identical conditions.